



## Cholesterol favors the anchorage of human dystrophin repeats 16 to 21 in membrane at physiological surface pressure



Sarah Ameziane-Le Hir<sup>a,b,c,d</sup>, Céline Raguénès-Nicol<sup>a,c,d</sup>, Gilles Paboeuf<sup>a,b,d</sup>, Aurélie Nicolas<sup>a,c,d</sup>, Elisabeth Le Rumeur<sup>a,c,d</sup>, Véronique Vié<sup>a,b,d,\*</sup>

<sup>a</sup> Université de Rennes 1, 35042 Rennes, France

<sup>b</sup> UMR CNRS 6251, Institut de physique de Rennes, Campus Beaulieu, F-35042 Rennes, France

<sup>c</sup> UMR CNRS 6290, Equipe SIM, Campus Villejean, F-35043 Rennes, France

<sup>d</sup> Université Européenne de Bretagne, 5 boulevard Laënnec, F-35000 Rennes, France

### ARTICLE INFO

#### Article history:

Received 5 July 2013

Received in revised form 7 January 2014

Accepted 10 January 2014

Available online 16 January 2014

#### Keywords:

Atomic force microscopy

Langmuir film

Muscular dystrophy

Protein lipid interaction

CRAC sequence

Spectrin superfamily

### ABSTRACT

Dystrophin (DYS) is a filamentous protein that connects the cytoskeleton and the extracellular matrix via the sarcolemma, conferring resistance to muscular cells. In this study, interactions between the DYS R16–21 fragment and lipids were examined using Langmuir films made of anionic and zwitterionic lipids. The film fluidity was modified by the addition of 15% cholesterol. Whatever the lipid mixture examined, at low surface pressure (20 mN/m) few differences appeared on the protein insertion and the presence of cholesterol did not affect the protein/lipid interactions. At high surface pressure (30 mN/m), the protein insertion was very low and occurred only in zwitterionic films in the liquid-expanded phase. In anionic films, electrostatic interactions prevented the protein insertion outright, and caused accumulation of the protein on the hydrophilic part of the monolayer. Addition of cholesterol to both lipid mixtures drastically modified the protein–lipid interactions: the DYS R16–21 insertion increased and its organization in the monolayer appeared to be more homogeneous. The presence of accessible cholesterol recognition amino-acid consensus sequences in this fragment may enhance the protein/membrane binding at physiological lateral pressure. These results suggest that the anchorage of dystrophin to the membrane *in vivo* may be stabilized by cholesterol-rich nano-domains in the inner leaflet of sarcolemma.

© 2014 Elsevier B.V. All rights reserved.

### 1. Introduction

Dystrophin (DYS) is a long filamentous muscular protein of 427 kDa (about 175 nm long) [1,2]. Most of this length is due to a long central rod domain composed of 24 spectrin-like repeats (R1 to R24) folded into a triple- $\alpha$ -helical bundle [3]. The biological function of dystrophin is to protect the membrane against stress during elongation/contraction muscular cycles. Its absence leads to the severe disease Duchenne muscular dystrophy (DMD), whereas the milder Becker muscular dystrophy (BMD) may be observed when truncated proteins are expressed [4]. Due to its high levels of STRs, dystrophin is a member of the spectrin-like superfamily [5]. A relationship has been suggested between the structural organization of the repeat domains in these proteins and the membrane's protection against shearing stresses [3]. This function may result from a homogeneous protein distribution along the membrane caused by protein/lipid interactions. Indeed, spectrin is known to bind to the inner membrane leaflet due to interactions with

phosphatidylserine [6–9]. Moreover the presence of 10–20% cholesterol (CHOL) facilitates the insertion of spectrin into phosphatidylethanolamine/phosphatidylcholine monolayers that were performed at low surface pressure, i.e. from 8 to 11 mN/m [10]. Even during its liquid-expanded phase (LE), spectrin binding capacity depends on the fluidity of the monolayer. Our previous studies showed that fragments of the dystrophin rod domain interact with membrane system models through electrostatic and/or hydrophobic forces [11,12].

This study is focused on the interaction of the specific dystrophin fragment made of repeats R16 to R21 and a membrane model. This construct has several specific features that set it apart from other dystrophin fragments. For instance, it contains a hinge (H3) between the repeats R19 and R20 [13,14]. The presence of H3 in microdystrophin improves the capacity for muscle degeneration prevention, while deletion of this hinge leads to the BMD phenotype [15,16]. In addition, DYS R16–21 is coded by exons 42 to 53, which includes the hot-spot between exons 45 and 53 where about one third of BMD patients have mutations [17]. The fragment also mediates specific protein interactions, such as the anchoring of neuronal NO Synthase (nNOS) to the sarcolemma through R16–R17 [18]. The mislocalisation of nNOS in the membrane leads to a decrease of muscular strength in dystrophin-

\* Corresponding author at: 263 av. du général Leclerc, Université de Rennes 1, Institut de Physique de Rennes, Bat 11A, 35042 Rennes cedex, France.

E-mail address: [Veronique.vie@univ-rennes1.fr](mailto:Veronique.vie@univ-rennes1.fr) (V. Vié).

deficient *mdx* mice [19]. R16–21 is located in the last part of the protein, where the cysteine-rich domain is known to bind to  $\beta$ -dystroglycan ( $\beta$ -DG) in a membrane protein complex [20] that is located in detergent-resistant membrane. Sarcolemmal CHOL depletion induces the weakening of force contractions through the redistribution of  $\beta$ -DG, and is accompanied by a reduction of  $\beta$ -DG/dystrophin interactions in favor of  $\beta$ -DG/caveolin-3 interactions [21]. All these studies showed that structural or lipid environmental modifications impact muscular activity. Nevertheless, up to now little was known about the ability of DYS R16–21 to interact with lipid membranes.

Here, we address the question of the DYS R16–21 anchorage in mixed lipid films and more particularly of the effect of CHOL on the interaction. Since phosphatidylserine is specifically abundant in the inner leaflet of the sarcolemma membrane, the effect of the polar head charge was tested using a simplified mixture composed of anionic dioleoylphosphatidylserine (DOPS) and zwitterionic dioleoylphosphatidylcholine (DOPC) lipids. Because we chose unsaturated lipids, the monolayers are in the LE phase regardless of the surface pressure. A mix of dipalmitoylphosphatidylcholine (DPPC) and DOPC was used to mimic a detergent-resistant membrane as described [22,23]. Indeed DPPC has been reported to form liquid-condensed (LC) phase domains and also to create separated phases when mixed with DOPC [24]. Cholesterol, also present in the inner leaflet up to 25% [25], is known to modulate membrane fluidity, and particularly at high surface pressure, it acts as a head group spacer because of its molecular orientation in the monolayer. Moreover, CHOL is located mainly in the condensed phase formed by DPPC [26,27]. Langmuir monolayers were used, which allowed for control of charge densities, of fluidity, and of lipid packing according to specific lipid compositions and surface pressures. Protein–lipid interactions and protein structure were determined by combining tensiometric and ellipsometric measurements with atomic force microscopy imaging. We evaluated the influence of 15% CHOL on the interaction of DYS R16–21 with DOPC/DOPS and DOPC/DPPC lipid mixtures. Using two initial surface pressures, two different lipid packings were tested. The highest of these (30 mN/m) is considered to be comparable to physiological membrane pressure [28,29].

Our results show that DYS R16–21 interacts with the lipid monolayer no matter what mixture was used, while the surface pressure has a notable impact on the insertion. In addition, under high surface pressure CHOL was shown to stabilize the fragment at lipid interface, likely through the presence of two cholesterol recognition amino-acid consensus (CRAC) sequences on the protein surface [30]. The presence of CRAC sequences all along dystrophin allows specific protein/lipid interactions that result in homogeneous protein distribution along the membrane. This anchorage could be related to lateral force transmission during muscle elongation/contraction.

## 2. Experimental sections

### 2.1. Materials

All lipids were purchased from Avanti Polar Lipids (Alabama, US). The pGEX-4T-1 plasmid vector and GSTrap HP and Sephacryl S-100 columns were bought from GE Healthcare. BL21 bacteria and restriction enzymes were purchased from Ozyme (St.-Quentin-en-Yvelines, France). Purified bovine thrombin came from Stago (Asnières-sur-Seine, France).

### 2.2. Preparation of recombinant DYS R16–21 protein

The DYS R16–21 fragment begins at residue Ser 1994 and ends with Thr 2686, using the full-length human dystrophin annotation (NCBI NP\_003997). In order to improve stability and as previously done for other dystrophin fragments [31,32], we included a three-amino-acid extension in the N-terminus and a seven-amino-acid extension in the

C-terminus. The protein was cloned in pGEX-4T-1 then expressed in a protease-deficient *Escherichia coli* BL21 strain as a GST-tagged protein [33]. Cell lysis was obtained by sonication after lysozyme treatment. DYS R16–21 was further purified using GST affinity chromatography. After thrombin proteolysis (50 UI for 2 h at room temperature), the chromatography fractions were separated by salting-out with ammonium sulfate. The target protein was collected at 24% salt saturation and rediluted in TNE buffer (20 mM Tris, 150 mM NaCl, 0.1 mM EDTA, pH 7.5). Purification was achieved with size-exclusion chromatography by passing it through a Sephacryl S-100 column (L 2.6 cm  $\times$  H 60 cm) at 1 mL/min using the same buffer. After purification, the protein was concentrated using a 30 kDa cut-off centrifugal concentrator. Purity was assessed by 10% SDS-Polyacrylamide gel electrophoresis (SDS-PAGE), and concentration was determined using a bicinchoninic acid assay with a standard of serum albumin.

Circular dichroism spectra were acquired between 250 nm and 200 nm, with 1.5  $\mu$ M of protein in TNE buffer at 20 °C (J-815, Jobin-Yvon) using 0.2 cm path-length cells. The  $\alpha$ -helical content was calculated from the mean molar residue ellipticity  $[\theta]$  ( $\text{mdeg.cm}^2.\text{dmol}^{-1}$ ) at 222 nm [34].

### 2.3. Tensiometric and ellipsometric measurements

In order to investigate the interfacial properties of the protein with and without lipids, surface pressure and ellipsometric angles were measured in Teflon troughs (4, 8, or 60 mL) at 20 °C. The Wilhelmy method was used to determine the surface pressure using a tensiometer (Nima Technology, Cambridge, UK). Ellipsometric measurements were performed with a conventional polarizer–analyzer null-ellipsometer setup. Briefly, a He–Ne laser (632.8 nm; Melles Griot, Carlsbad, CA) with an angle of incidence of 52.18° (1° away from the Brewster's angle), was used as the light source. Reflecting surface properties were explored by recording the positions of the polarizer and analyzer having the minimal intensity of transmitted light. The analyzer angle was doubled to yield the value of the ellipsometric angle ( $\Delta$ ) [35–37]. Both  $\Delta$  and the surface pressure ( $\pi$ ) were recorded as functions of time. The amphiphilic character was determined by reporting the surface pressure reached at this end of the absorption kinetics as a function of the protein's subphase concentrations (ranging from 0.0001  $\mu$ M to 1  $\mu$ M). For lipid/protein experiments, the lipid mixtures (DOPC/DOPS 1:1 molar ratio and DOPC/DPPC 1:1 molar ratio) were prepared in a 2:1 chloroform/methanol solution (v/v) at 0.5 mM, and where used, CHOL was added at 15% (molar ratio). The lipids were gently spread at the air/liquid interface of the TNE subphase at the desired surface pressure. These initial lipid surface pressures ( $\pi_i$ ) ranged from 5 to 35 mN/m. At a final concentration of 0.03  $\mu$ M, the protein was then injected into the subphase just beneath the lipid monolayer. The variations ( $\delta\Delta$  and  $\Delta\pi$ ) induced by protein adsorption at the end of the absorption kinetics were reported as functions of time and  $\pi_i$ . Each experiment was repeated up to four times and means  $\pm$  standard deviation (SD) were provided for each series. The temperature varied between 19 and 21 °C.

### 2.4. Atomic force microscopy (AFM) observations

The interfacial film was transferred onto a freshly-cleaved mica plate using the Langmuir–Blodgett technique. The experiment was realized using a 102 cm<sup>2</sup> Langmuir trough equipped with two movable barriers and controlled by a computer (model 601 M, Nima Technology, Cambridge, UK). The transfer was performed at the end of the kinetics and at a constant surface pressure. The dipper speed rate was 1 mm/min. Transferred monolayers were imaged using a PicoPlus atomic force microscope (Agilent Technologies, Phoenix, AZ) equipped with a 10  $\mu$ m scanner operating in contact mode. Images were acquired under ambient conditions using silicon nitride tips on integral cantilevers (ScienTec) with a spring constant of 0.06 N/m. For each measurement, the set point was adjusted before and during the scanning to minimize

the force between the tip and the sample. In each case, images were obtained from at least two samples prepared on different days, with at least four macroscopically-separated areas in each sample. To determine the height of the objects, after processing the images with Gwyddion 2.26 software (<http://gwyddion.net>) we did a statistical analysis. Objects of interest were selected by threshold, and then areas and maximal heights were determined. The values of height versus area were plotted, resulting in a plateau. This plateau included the majority of the objects and was used to compare the different experimental conditions.

### 2.5. Three-dimensional molecular homology modeling and surface properties

Three-dimensional (3D) homology models were obtained using I-TASSER server [38]. As previously described [39], the sequences of two successive repeats (“tandem repeats”) with an overlap of a single repeat were submitted to I-TASSER (e.g. DYS R16–17, then DYS R17–18, and so on). The H3 sequence was submitted separately. Superposition of the shared repeat of two successive tandem repeats allowed the construction of an extended model which we further minimized by YASARA (e.g. the DYS R16–17 and DYS R17–18 models were used to construct a DYS R16–18 model). In this way, step by step, the global 3D structure was reconstructed. Surface hydrophobicity was calculated using PLATINUM [40] and surface electrostatic potentials in the presence of 50 mM NaCl were calculated using the Adaptive Poisson–Boltzmann Solver (APBS) software [41]. Visualization was done using VMD and PyMOL.

## 3. Results

### 3.1. Protein purification

SDS-PAGE of the recombinant human dystrophin fragment DYS R16–21 (Fig. 1A) showed the protein at the expected molecular weight of 80 kDa. As expected with spectrin-like repeats [11,42], the circular dichroism spectrum of DYS R16–21 displayed the typical predominant  $\alpha$ -helix folding with two minima at 208 and 222 nm (Fig. 1B). Per Chen et al., the molar ellipticity of 222 nm allowed for determination of an  $\alpha$ -helix content of 83% [43]. The ratio of the molar ellipticity at 222 and 208 nm ( $\theta_{222}/\theta_{208}$ ) was 1.05, indicating that the helices were interacting and folded in a coiled-coil [44]. Therefore, it appears that the recombinant DYS R16–21 fragment was highly purified and correctly folded, conditions necessary for its further study.

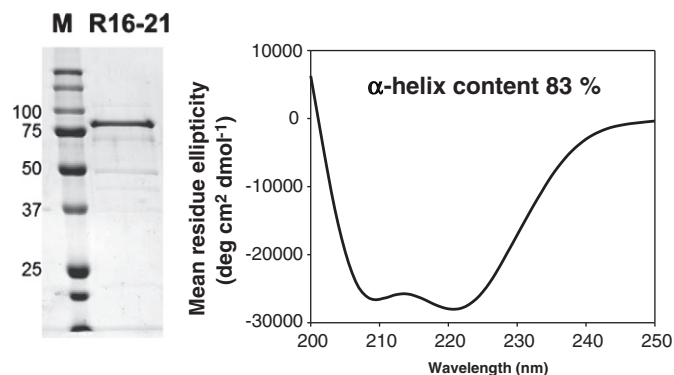


**Fig. 1.** DYS R16–21 sub-domain purification and secondary structure analysis. (left) 10% SDS polyacrylamide gel of DYS R16–21 obtained after purification. Lane M is the protein ladder. (right) Circular dichroism measurements of 1.5  $\mu$ M of DYS R16–21 in TNE buffer (pH 7.5) at 20 °C.

### 3.2. Amphiphilic properties of DYS R16–21

For each DYS R16–21 subphase concentration between 0.0001 and 1  $\mu$ M, surface pressure measurements were done and the final surface pressure versus subphase protein concentrations are reported in Fig. 2A. As the protein concentration increased,  $\pi$  increased until a plateau ( $\pi_{\text{max}}$ ) of 21 mN/m was reached, indicating the amphiphilic character of DYS R16–21. From these adsorption kinetic results, the critical concentration required for interface saturation was determined to be 0.1  $\mu$ M. For further experiments, a protein concentration of 0.03  $\mu$ M (or 2.5  $\mu$ g/mL) was chosen (indicated with an arrow in Fig. 2A) to avoid a potential aggregation of proteins in the subphase or the formation of multilayers at the interface. Fig. 2B shows a typical adsorption time for this protein concentration. Whereas surface pressure is related to the protein's ability to cover the interface and to interact laterally, the ellipsometric angle depends on the amount of matter at the interface. As is usual, at the very beginning of the adsorption the ellipsometric angle increased quicker than the surface pressure. It reached an angle of 10° at equilibrium, a value corresponding to a monolayer as experienced in other proteins [45]. AFM imagery of this monolayer at the end of the adsorption kinetics (Fig. 2C) showed a homogeneous film with no aggregation.

### 3.3. DYS R16–21 interaction with lipid monolayers

The adsorption kinetics of DYS R16–21 was monitored at various initial lipid surface pressures ( $\pi_i$ ). The variations of the surface pressure ( $\Delta\pi$ ) i.e. the difference between the initial lipid surface pressure and the final surface pressure were reported as a function of  $\pi_i$  (Fig. 3). When  $\pi_i$  increased,  $\Delta\pi$  induced by adsorption of DYS R16–21 decreased. Indeed as the lipids compacted, the protein was less and less able to be inserted into the lipid monolayer. When there was no more variation between the initial and final surface pressures ( $\Delta\pi = 0$  or intercept of the linear regression with the x axis as indicated with arrows in Fig. 3), the maximal insertion pressure (MIP) was reached [46]. This was clearly dependent on the lipid mixture, with values of 26.5 mN/m for DOPC/DOPS and 33 mN/m for DOPC/DPPC.

For  $\pi_i$  less than 20 mN/m,  $\Delta\pi$  was higher with anionic than with zwitterionic lipids, suggesting an attractive role for electrostatic interactions in the insertion of DYS R16–21. On the other hand, when  $\pi_i$  was higher than 20 mN/m,  $\Delta\pi$  was higher with zwitterionic lipids, suggesting presence of hydrophobic interactions during the protein's insertion process, while electrostatic interactions limit the insertion. Moreover, for the DOPC/DOPS monolayer at an initial surface pressure higher than  $\pi_e$  (26 mN/m), the protein induced a surface pressure decrease ( $\Delta\pi = -1.6$  mN/m), thus showing that attractive interactions were still taking place between DYS R16–21 and the compacted DOPC/DOPS monolayer.

To further analyze the organization of DYS R16–21 in lipid environments, we focused our work on lipid monolayers formed at two significant initial surface pressures: 20 mN/m, where the protein adsorption induced similar overpressures for all lipid compositions tested; and 30 mN/m, considered to be close to physiological membrane pressure [29]. All reported values are recapitulated in Table S1.

### 3.4. Cholesterol has few effects at a $\pi_i$ of 20 mN/m

Cholesterol is known to influence lipid packing therefore we studied the impact of 15% CHOL on the DYS R16–21/lipid interactions. At  $\pi_i$  of 20 mN/m (Fig. 4A), no changes were observed upon the addition of CHOL to the DOPC/DOPS film, while there was a slight increase of  $\Delta\pi$  and  $\delta\Delta$  (1 mN/m and 0.4° respectively) in the DOPC/DPPC mixture. AFM images of pure lipid films were unmodified in the presence of CHOL. DOPC/DOPS  $\pm$  CHOL (Fig. 4B) formed a homogeneous liquid-expanded (LE) phase. DOPC/DPPC  $\pm$  CHOL images (Fig. 4E) showed the coexistence of an LE phase of DOPC and a liquid-condensed (LC)

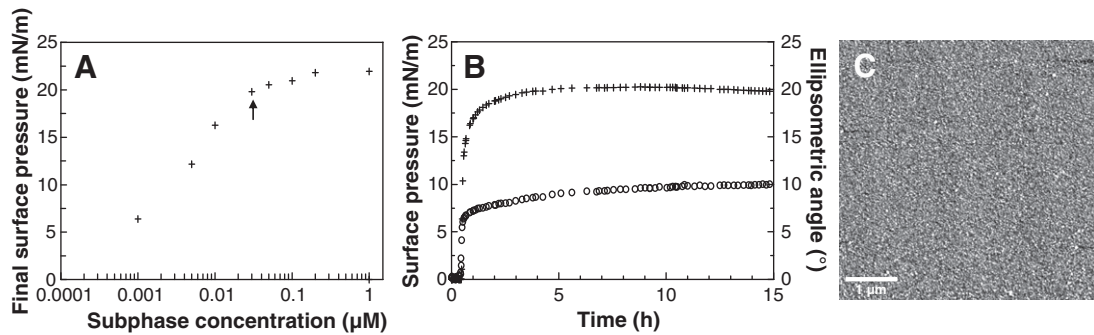


**Fig. 2.** DYS R16–21 adsorption at the air–liquid interface. (A) Final surface pressure reached at the end of the adsorption kinetics versus DYS R16–21 subphase concentrations. Arrow indicates  $\pi$  reached for protein subphase concentration of 0.03  $\mu\text{M}$ . (B) Adsorption kinetics of DYS R16–21 at air–liquid interface for the subphase concentration of 0.03  $\mu\text{M}$ , surface pressure (+), and ellipsometric angle (o). (C) AFM topographic image of transferred DYS R16–21 monolayer at the end of the kinetics (5 h). Surface pressure was 20 mN/m. Scan size 5  $\mu\text{m} \times 5 \mu\text{m}$ , z scale 10 Å.

phase of DPPC, as previously observed [47]. The LC domains were several  $\mu\text{m}$  in diameter and their apparent height was  $1.4 \pm 0.1 \text{ nm}$ .

Mixed protein/lipid films showed bright protrusions attributed to the protein's presence (Fig. 4C–H). In DOPC/DOPS  $\pm$  CHOL films, these protrusions appeared mostly as worm-like curved filaments (Fig. 4C–D). CHOL induced both protein clustering and an increase in the apparent height of protrusions ( $2.1 \pm 0.1 \text{ nm}$  without CHOL versus  $2.7 \pm 0.1 \text{ nm}$  with CHOL). These changes in DYS R16–21 organization occurred even though the lateral pressure and the amount of material at the interface were similar with or without CHOL (Fig. 4A).

In DOPC/DPPC films (Fig. 4E–H), the presence of DYS R16–21 drastically decreased the LC domain's diameter, which never exceeded 400 nm. Without CHOL (Fig. 4 F–G), the proteins appeared as round objects or filaments with heights higher ( $2.0 \pm 0.1 \text{ nm}$ ) than those of LC domains ( $1.4 \pm 0.1 \text{ nm}$ ). The filaments were most often stuck to an LC phase (detailed view, Fig. 4G) whereas round objects were located in an LE phase. In the presence of CHOL (Fig. 4H), higher filaments ( $3.1 \pm 0.2 \text{ nm}$ ) were located both in the LE phase and at the boundaries of LE/LC phases.

### 3.5. Cholesterol increases DYS R16–21 insertion at a $\pi_i$ of 30 mN/m

Ellipsometric and tensiometric measurements (Fig. 5A) showed that in any lipid condition, a  $\pi_i$  of 30 mN/m induced the presence of less protein at the interface than with a  $\pi_i$  of 20 mN/m. Injection of DYS R16–21 under the DOPC/DOPS/CHOL monolayer led to an increase in surface pressure (from  $-1.6 \text{ mN/m}$  without CHOL to  $+2 \text{ mN/m}$  with CHOL) and a decrease in the ellipsometric angle (from  $0.6^\circ$  without CHOL to  $0.2^\circ$  with CHOL), indicating modified protein/lipid interactions

that favor the insertion of DYS R16–21. In the DOPC/DPPC films, the presence of CHOL had no significant effects on ellipsometric angle variation after injection of DYS R16–21, whereas the presence of CHOL induced an increase in  $\Delta\pi$  (from 0.3 mN/m without CHOL to 2 mN/m).

The AFM images of DOPC/DOPS films with or without CHOL (Fig. 5B) were similar to those at 20 mN/m. The DOPC/DPPC/CHOL AFM images revealed that the presence of CHOL caused a slight decrease in height of LC domains (from 1.4 nm without CHOL to 1.2 nm) (Fig. 5E).

In the DOPC/DOPS/protein films (Fig. 5C), DYS R16–21 appeared as protrusions forming heterogeneous clusters higher ( $3.6 \pm 0.4 \text{ nm}$ ) and larger than those previously observed at a  $\pi_i$  of 20 mN/m. This is consistent with the variations in surface pressures and ellipsometric angles seen with the two surface pressures (Figs. 4A and 5A). In the presence of CHOL (Fig. 5D), the proteins formed small protrusions that are smaller in length, width, and height ( $2.3 \text{ nm} \pm 0.1$ ) than those in the absence of CHOL or with a smaller  $\pi_i$ . Finally, the protein organization was more homogeneous, with deeper insertion into the lipid monolayer and less material at the interface.

In DOPC/DPPC/protein films (Fig. 5F), the protein was present as scarce clusters in agreement with the low  $\Delta\pi$ . Their heights (between 1 and 4 nm), were very heterogeneous. By contrast, CHOL induced numerous clusters of DYS R16–21 (Fig. 5G–H) with heights of  $2.6 \pm 0.2 \text{ nm}$ . The LC domain borders were much more irregular and angular than without CHOL. The protein clusters appear to be more elongated when in contact with LC domains than when embedded in LE domains (detailed view, Fig. 5H). Some objects also appeared to be embedded in LC domains, but since there was a depression surrounding these clusters it was obvious that there was no direct contact between the LC and the protein.

### 3.6. Computational analysis of DYS R16–21 in presence of 50 mM NaCl

As expected for a soluble protein, the molecular surface of DYS R16–21 is mainly hydrophilic. Nevertheless one side of the fragment displays a higher presence of hydrophobic amino acids (Fig. 6). The electrostatic potential at the molecular surface shows a distribution of negative and positive charges along the molecule. Numerous positive patches were observed, mainly on repeats 16 and 17 of DYS R16–21, with the rest dispersed more widely along the molecule and embedded in the negative surface. A rotated view of the fragment showed a more contrasted surface with larger negative patches, separated by a few small positive zones that appear mostly on repeats 18 and 19. Interestingly, some hydrophobic patches colocalize or are very close to the cationic surface (for example on R16, R18 and R20). These may thus be anchorage points for interaction or insertion in anionic and zwitterionic lipid monolayers even under high initial surface pressures.

A search of the primary sequence of dystrophin revealed several occurrences of the CRAC pattern  $-(L/V)-(X)_{1-5}-Y-(X)_{1-5}-(R/K)-[30]$ . Due to this sequence, a cholesterol binding cleft is created where Y

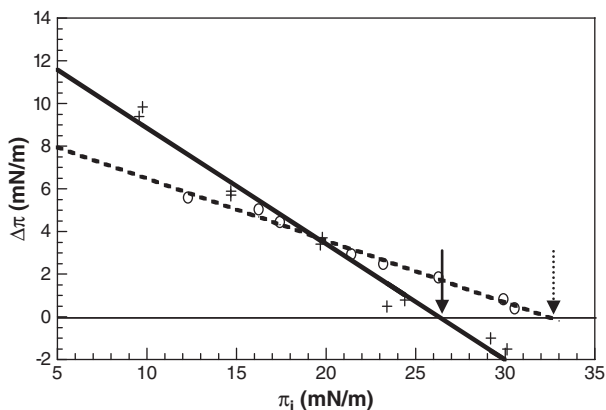


**Fig. 3.** Overpressure induced by adsorption of DYS R16–21 at air/lipid interface versus the initial lipid surface pressures of DOPC/DOPS (full line) and DOPC/DPPC (dotted line). Arrows indicate the values of maximal insertion pressures (MIP). The subphase concentration of DYS R16–21 was 0.03  $\mu\text{M}$ .

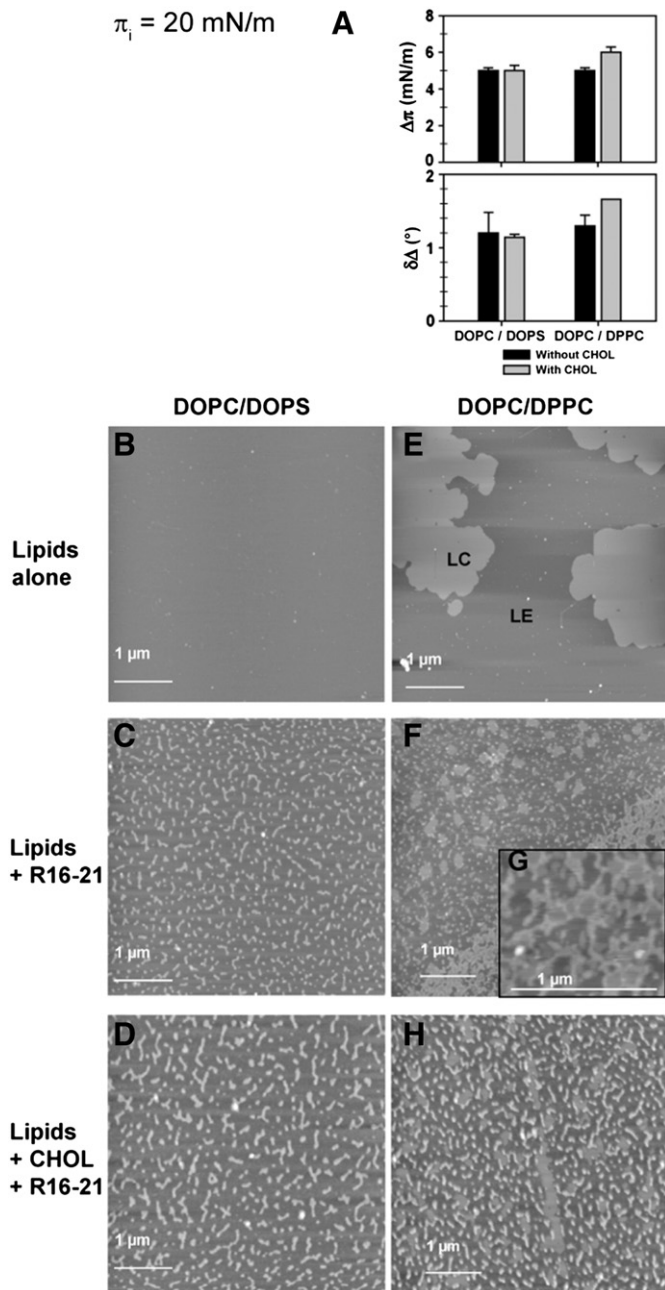


**Fig. 4.** Characterization of DYS R16–21 at the initial lipid surface pressure of 20 mN/m. (A) Variations of the surface pressure ( $\Delta\pi$ ) and of the ellipsometric angle ( $\delta\Delta$ ) induced by DYS R16–21 adsorption on phospholipid monolayers (black) and phospholipid/CHOL monolayers (gray). (B–H) Typical AFM topographic images of monolayers as indicated on the panels. Scan size  $5 \mu\text{m} \times 5 \mu\text{m}$  for images B–F and H, and  $2 \mu\text{m} \times 2 \mu\text{m}$  for image G. Z-range 80 Å. When present, DYS R16–21 subphase concentration is 0.03  $\mu\text{M}$ , CHOL 15%. LE, liquid-expanded phase; LC, liquid-condensed phase.

and R/K interact directly with CHOL [48]. In DYS R16–21, the pattern was found in the C helix of R16 ( $V_{2088}NKMYKDR_{2098}$ ) and in the R21 B–C loop ( $L_{2647}RDYSADDTR_{2657}$ ) (Fig. 6). Most of the amino acids involved are exposed on the surface, and accessible enough to enable interaction with CHOL molecules.

#### 4. Discussion

In this study, we examine the interaction of DYS R16–21 with lipid monolayers. This particular dystrophin fragment is characterized by the presence of hinge 3 (H3) and is frequently mutated in patients. DYS R16–21 displayed amphiphilic properties that were probably due

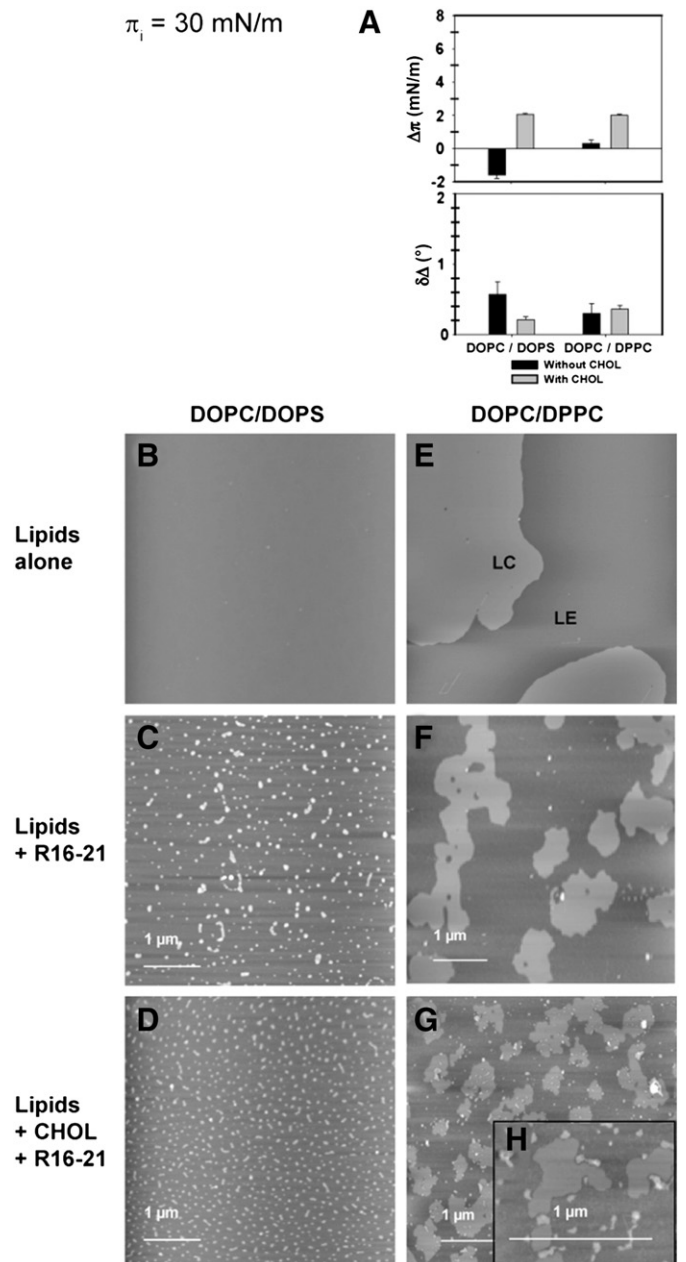


**Fig. 5.** Characterization of DYS R16–21 at an initial lipid surface pressure of 30 mN/m. (A) Variations of the surface pressure ( $\Delta\pi$ ) and of the ellipsometric angle ( $\delta\Delta$ ) induced by DYS R16–21 adsorption on phospholipid (black) and phospholipids/CHOL monolayers (gray). (B–H) Typical AFM topographic images of monolayers as indicated on the panels. Scan size  $5 \mu\text{m} \times 5 \mu\text{m}$  for images B–G and  $2 \mu\text{m} \times 2 \mu\text{m}$  for image H. Z-range 80 Å. When present, DYS R16–21 subphase concentration is 0.03  $\mu\text{M}$  and CHOL, 15%. LE, liquid-expanded phase; LC, liquid-condensed phase.

to the presence of hydrophobic amino-acids all along the surface (Fig. 6). Compared with previously-studied rod domain fragments, the adsorption of DYS R16–21 at the air/water interface was faster, the plateau was reached at a smaller protein concentration but has a similar value of 21 mN/m [12,49]. This indicates both that the interface is more rapidly covered by the protein, and that the molecules do indeed interact with each other. This result could be related to the larger size of the protein as compared to other dystrophin fragments previously studied, and/or to the presence of H3, which may make the protein's structure more flexible [13].

The monolayer's initial lipid surface pressure ( $\pi_i$ ) is a major factor influencing the adsorption of amphiphilic proteins through electrostatic or hydrophobic forces because it determines lipid packing. When  $\pi_i$  was

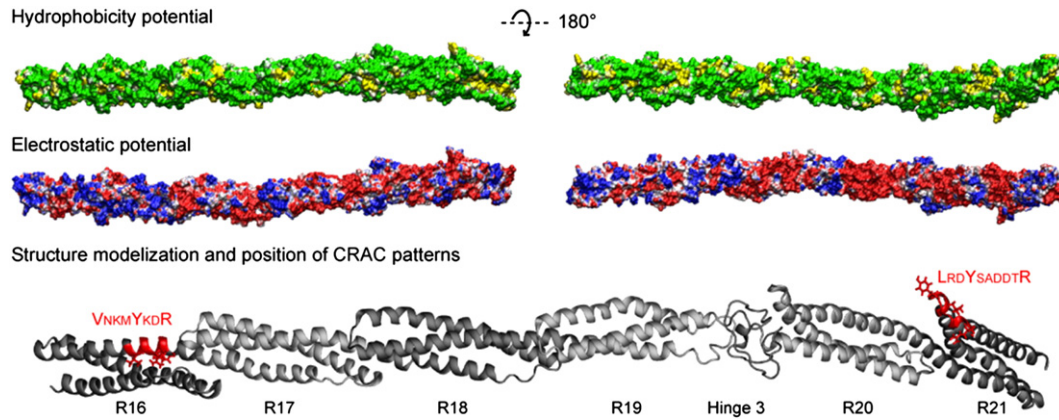


**Fig. 6.** Molecular modeling of DYS R16–21. The 3D structure of DYS R16–21 was created in I-TASSER. The hydrophobic potential at the molecular surface (top row) is colored by increasing hydrophobicity from green (polar) to yellow (hydrophobic). The electrostatic potential at the molecular surface (middle row) is colored by increasing levels from red (–) to blue (+). The N-terminus (R16) is located at the left of the molecules. Left and right images in the top rows are representations of a 180°-rotation along the molecule's long axis. Bottom row: 3D structure of DYS R16–21 in cartoon representation. Each dystrophin repeat is a different gray. Amino acids of the CRAC (cholesterol recognition/interaction amino acid consensus) patterns are red.

below 20 mN/m, the protein was able to insert itself into both anionic and zwitterionic monolayers; however the maximal insertion pressure was significantly lower for the anionic mixture suggesting that attractive electrostatic interaction plays a major role in DYS R16–21–membrane interactions. The negative charge of the polar head attracts the protein toward the membrane, allowing further hydrophobic interactions to occur thanks to free interfacial space. At a  $\pi_i$  of 20 mN/m, the protein insertion overpressures and ellipsometric angle variations seem to be equivalent for both lipid mixes. AFM observations show the protein as round or fibrous objects with regular heights (about one protein thick). The fibrous objects were present in the anionic mix, and interconnected filaments were only detected in contact with LC domains. These features imply that the molecules were stabilized at the interface by negative charges or LC domains and then adopted the same orientation at the lipid interface. This favors the existence of lateral protein/protein interactions in both lipid mixtures. At a  $\pi_i$  over 20 mN/m, electrostatic interactions still occur but the space between lipid head groups becomes more and more limited, and the fragment insertion slows. Finally, when the  $\pi_i$  of the DOPC/DOPS film was over 26 mN/m, interactions with lipid head groups caused a reorientation and relaxation of the films, as shown by a decrease in the final surface pressure, and the protein appears as irregular clusters. This phenomenon has been reported previously for the dystrophin R2 repeat [50], DYS R20–24 [12] and in  $\alpha$ -spectrin [6]. In zwitterionic film, however, the insertion of DYS R16–21 occurs up to 31 mN/m. This is probably because the protein's orientation is not driven by electrostatic interactions and because its flexibility allows for penetration of the films even at higher surface pressures.

When comparing the anionic monolayer insertion of the previously-studied fragments DYS R1–3, DYS R11–15 and DYS R20–24 to that of the DYS R16–21 studied here, different behaviors are seen, thus demonstrating that these fragments are not interchangeable as had been stated [51]. Indeed, at 30 mN/m, only DYS R11–15 inserts into the monolayer ( $\Delta\pi = +2$  mN/m) [49], whereas both DYS R16–21 and R20–24 stayed at the head group level [12].

At 20 mN/m, a gradient seems to occur along the central domain, with greater insertion for fragments from the N- to C-terminal ends ( $\Delta\pi = 7$  mN/m for DYS R1–3, 6 mN/m for DYS R11–15, and 5 mN/m for DYS R16–21 and DYS R20–24). This intriguing observation must be further studied to decipher whether it has a physiological significance. It would be especially interesting to understand the relationship between the variation in sarcolemmal lateral pressure during muscle elongation/contraction, and the number or position of anchoring points along the protein. Interestingly, it has been reported that binding of spectrin to phosphatidylserine in the inner membrane increases the mechanical stability of red blood cell membranes [52].

We examined dystrophin/lipid/CHOL interactions because of cholesterol presence in the membrane and of its impact on the membrane's physical properties. Moreover we report the existence of a specific amino-acid sequence called CRAC (cholesterol recognition amino-acid consensus) and involved in CHOL binding [30,53]. Like spectrin [54,55], dystrophin has been shown to be associated in vivo to detergent-resistant membranes [56] and the interaction between  $\beta$ -DG and dystrophin is weakened by CHOL depletion [21]. The impact of CHOL on the structural and lateral organization of lipid layers is highly-documented [27,57,58], in particular its role as head group spacer and its usual localization in the condensed phase formed by DPPC [26]. In addition, several monolayer experiments have shown complex formation between CHOL and phosphatidylserine, an important component of the inner leaflet [59]. Our study was performed at 15% of CHOL since 10 to 20% CHOL have been shown to increase spectrin insertion in phosphatidylethanolamine/phosphatidylcholine monolayers [10] and also because this concentration is known to preserve lateral phase separation [60]. At the lower initial surface pressure (20 mN/m), macroscopic measurements ( $\pi$ ,  $\Delta$ ) were unmodified in presence of CHOL, but topographic images revealed an increase in the lateral size and height of protein protrusions, indicating changes in the molecular organization of DYS R16–21 within the lipid monolayers. CHOL favors lateral protein–protein interactions, and since the lipids are in fluid phase, it increases steric packing in the hydrophobic part, limiting deep anchoring. In the DOPC/DPPC mixture, LC domain fragmentation is induced by the protein. DYS R16–21 insertion might induce local disorders in the lateral packing of the acyl chains. These hydrophobic mismatch defects result in lateral fragmentation of these domains, and this phenomenon is amplified by the presence of CHOL [61,62]. At a higher initial surface pressure ( $\pi_i = 30$  mN/m), CHOL amplifies protein insertion into lipid monolayers and favors a homogeneous organization of the protein in both LC and LE domains. Indeed, the sterol polar head group is small compared to choline or serine, while the hydrophobic part at this pressure is similar to that of a phosphatidylcholine-saturated chain [24], thus CHOL plays the role of head group spacer. This promotes a deeper and more homogeneous lipid insertion. The DOPS/DYS R16–21 electrostatic interactions are modified by CHOL. This could be linked either to PS/CHOL complex formation as suggested by Radhakrishnan et al. [59] or to specific DYS R16–21/CHOL interactions.

Bio-informatics analysis of the DYS R16–21 amino acid sequence revealed two occurrences of the CRAC sequence  $-(L/V)-(X)_{1-5}-Y-(X)_{1-5}-(R/K)-$  [30]. CRAC sequences are also present in spectrin and

in other dystrophin fragments (Table S2). These patterns in DYS R16–21 are easily accessible for interaction at the protein surface. Not only has CRAC been identified in many proteins that interact with cholesterol, but it has been more widely suggested to be related to protein propensity for interaction with cholesterol-rich lipid domains [63]. CRAC motifs are often reported in membrane proteins, but are compatible with peripheral proteins and were also reported in a secreted toxin [64].

## 5. Conclusion

Our results highlight the fact that dystrophin fragments, and here especially DYS R16–21, can interact directly with monolayers at high surface pressure, at low fluidity, and in the presence of anionic lipids. We further show that the presence of dystrophin close to the membrane is probably not due only to a link with  $\beta$ -DG but also thanks to its own sub-part membrane-binding properties. It has now to be tested whether our *in vitro* results may be transposed *in vivo*. Does formation of direct interactions between dystrophin and cholesterol-rich nanodomains stabilize the dystrophin/ $\beta$ -DG/sarcolemma in muscular cells? If so, cholesterol-rich domains in the inner sarcolemma layer could prevent ejection of dystrophin under surface pressure variations due to contraction/elongation cycles and contribute to sarcolemma resistance.

## Abbreviations

DOPC	dioleoylphosphatidylcholine
DPPC	dipalmitoylphosphatidylcholine
DOPS	dioleoylphosphatidylserine
CHOL	cholesterol
LE	liquid expanded
LC	liquid condensed
AFM	atomic force microscopy
DYS	dystrophin
$\beta$ -DG	$\beta$ -dystroglycan
CRAC	cholesterol recognition/interaction amino acid consensus

## Acknowledgement

Supported by grants from the AFM “association française contre les myopathies”, GIS BRESMAT – Conseil Régional de Bretagne, and FEDER, “Fond Européen pour le Développement Régional”. SAL was funded by the “Ministère de l’Enseignement Supérieur et de la Recherche”, AN was funded by the CNRS.

Authors thanks Biosit – Structure Fédérative de Recherche en Biologie-Santé de Rennes for circular dichroism facilities. Juliana Berland post-edited the English style.

## Appendix A. Supplementary data

Supplementary data to this article can be found online at <http://dx.doi.org/10.1016/j.bbamem.2014.01.010>.

## References

- [1] M. Koenig, E.P. Hoffman, C.J. Bertelson, A.P. Monaco, C. Feener, L.M. Kunkel, Complete cloning of the Duchenne muscular dystrophy (DMD) cDNA and preliminary genomic organization of the DMD gene in normal and affected individuals, *Cell* 50 (1987) 509–517.
- [2] F. Pons, N. Augier, R. Heilig, J. Leger, D. Mornet, J.J. Leger, Isolated dystrophin molecules as seen by electron microscopy, *Proc. Natl. Acad. Sci. U. S. A.* 87 (1990) 7851–7855.
- [3] M. Muthu, K.A. Richardson, A.J. Sutherland-Smith, The crystal structures of dystrophin and utrophin spectrin repeats: implications for domain boundaries, *PLoS. One.* 7 (2012) e40066.
- [4] M. Koenig, A.H. Beggs, M. Moyer, S. Scherpf, K. Heindrich, T. Bettecken, G. Meng, C.R. Muller, M. Lindlof, H. Kaariainen, et al., The molecular basis for Duchenne versus Becker muscular dystrophy: correlation of severity with type of deletion, *Am. J. Hum. Genet.* 45 (1989) 498–506.
- [5] K.S. Vishwanatha, Y.P. Wang, H.T. Keutmann, R.E. Mains, B.A. Eipper, Structural organization of the nine spectrin repeats of Kalirin, *Biochemistry* 51 (2012) 5663–5673.
- [6] W. Diakowski, A. Prychidny, M. Swistak, M. Nietubyc, K. Bialkowska, J. Szopa, A.F. Sikorski, Brain spectrin (fodrin) interacts with phospholipids as revealed by intrinsic fluorescence quenching and monolayer experiments, *Biochem. J.* 338 (Pt 1) (1999) 83–90.
- [7] R.I. MacDonald, Temperature and ionic effects on the interaction of erythroid spectrin with phosphatidylserine membranes, *Biochemistry* 32 (1993) 6957–6964.
- [8] R. Maksymiw, S.F. Sui, H. Gaub, E. Sackmann, Electrostatic coupling of spectrin dimers to phosphatidylserine containing lipid lamellae, *Biochemistry* 26 (1987) 2983–2990.
- [9] P.J. O’Toole, C. Wolfe, S. Ladha, R.J. Cherry, Rapid diffusion of spectrin bound to a lipid surface, *Biochim. Biophys. Acta* 1419 (1999) 64–70.
- [10] W. Diakowski, L. Ozimek, E. Bielska, S. Bem, M. Langner, A.F. Sikorski, Cholesterol affects spectrin–phospholipid interactions in a manner different from changes resulting from alterations in membrane fluidity due to fatty acyl chain composition, *Biochim. Biophys. Acta* 1758 (2006) 4–12.
- [11] S. Legardinier, C. Raguenes-Nicol, C. Tascon, C. Rocher, S. Hardy, J.F. Hubert, E. Le Rumeur, Mapping of the lipid-binding and stability properties of the central rod domain of human dystrophin, *J. Mol. Biol.* 389 (2009) 546–558.
- [12] V. Vie, S. Legardinier, L. Chieze, O. Le Bihan, Y. Qin, J. Sarkis, J.F. Hubert, A. Renault, B. Desbat, E. Le Rumeur, Specific anchoring modes of two distinct dystrophin rod sub-domains interacting in phospholipid Langmuir films studied by atomic force microscopy and PM-IRRAS, *Biochim. Biophys. Acta* 1798 (2010) 1503–1511.
- [13] M. Koenig, L.M. Kunkel, Detailed analysis of the repeat domain of dystrophin reveals four potential hinge segments that may confer flexibility, *J. Biol. Chem.* 265 (1990) 4560–4566.
- [14] N. Sahni, K. Mangat, E. Le Rumeur, N. Menhart, Exon edited dystrophin rods in the hinge 3 region, *Biochim. Biophys. Acta* 1824 (2012) 1080–1089.
- [15] G.B. Banks, L.M. Judge, J.M. Allen, J.S. Chamberlain, The polyproline site in hinge 2 influences the functional capacity of truncated dystrophins, *PLoS Genet.* 6 (2010) e1000958.
- [16] A. Carsana, G. Frisso, M.R. Tremolaterra, R. Lanzillo, D.F. Vitale, L. Santoro, F. Salvatore, Analysis of dystrophin gene deletions indicates that the hinge III region of the protein correlates with disease severity, *Ann. Hum. Genet.* 69 (2005) 253–259.
- [17] A. Nicolas, C. Lucchetti-Miganeh, R.B. Yaou, J.C. Kaplan, J. Chelly, F. Leturcq, F. Barloy-Hubler, E. Le Rumeur, Assessment of the structural and functional impact of in-frame mutations of the DMD gene, using the tools included in the eDystrophin online database, *Orphanet. J. Rare Dis.* 7 (2012) 45.
- [18] Y. Lai, G.D. Thomas, Y. Yue, H.T. Yang, D. Li, C. Long, L. Judge, B. Bostick, J.S. Chamberlain, R.L. Terjung, D. Duan, Dystrophins carrying spectrin-like repeats 16 and 17 anchor nNOS to the sarcolemma and enhance exercise performance in a mouse model of muscular dystrophy, *J. Clin. Invest.* 119 (2009) 624–635.
- [19] D. Li, Y. Yue, Y. Lai, C.H. Hakim, D. Duan, Nitrosative stress elicited by nNOS micro delocalization inhibits muscle force in dystrophin-null mice, *J. Pathol.* 223 (2011) 88–98.
- [20] J.M. Ervasti, Dystrophin, its interactions with other proteins, and implications for muscular dystrophy, *Biochim. Biophys. Acta* 1772 (2007) 108–117.
- [21] J. Vega-Moreno, A. Tirado-Cortes, R. Alvarez, C. Irls, J. Mas-Oliva, A. Ortega, Cholesterol depletion uncouples beta-dystroglycans from discrete sarcolemmal domains, reducing the mechanical activity of skeletal muscle, *Cell. Physiol. Biochem.* 29 (2012) 905–918.
- [22] J.H. Davis, J.J. Clair, J. Juhasz, Phase equilibria in DOPC/DPPC-d62/cholesterol mixtures, *Biophys. J.* 96 (2009) 521–539.
- [23] R.J. Schroeder, S.N. Ahmed, Y. Zhu, E. London, D.A. Brown, Cholesterol and sphingolipid enhance the Triton X-100 insolubility of glycosylphosphatidylinositol-anchored proteins by promoting the formation of detergent-insoluble ordered membrane domains, *J. Biol. Chem.* 273 (1998) 1150–1157.
- [24] X.M. Li, M.M. Momsen, J.M. Smaby, H.L. Brockman, R.E. Brown, Cholesterol decreases the interfacial elasticity and detergent solubility of sphingomyelins, *Biochemistry* 40 (2001) 5954–5963.
- [25] R.B. Gennis, *Biomembranes: Molecular Structure and Function*, Springer, 1988.
- [26] W. Guyer, K. Bloch, Phosphatidylcholine and cholesterol interactions in model membranes, *Chem. Phys. Lipids* 33 (1983) 313–322.
- [27] R.M. Epand, Cholesterol-rich domains: preface, *Biochim. Biophys. Acta Biomembr.* 1610 (2003) 155–156.
- [28] R. MacDonald, The relationship and interactions between lipid bilayers, vesicles, and lipid monolayers at the air/water interface, in: M. Rosoff (Ed.), *Vesicles*, CRC Press, New York, 1996, pp. 3–48.
- [29] D. Marsh, Lateral pressure in membranes, *Biochim. Biophys. Acta* 1286 (1996) 183–223.
- [30] H. Li, V. Papadopoulos, Peripheral-type benzodiazepine receptor function in cholesterol transport. Identification of a putative cholesterol recognition/interaction amino acid sequence and consensus pattern, *Endocrinology* 139 (1998) 4991–4997.
- [31] E. Kahana, P.J. Marsh, A.J. Henry, M. Way, W.B. Gratzner, Conformation and phasing of dystrophin structural repeats, *J. Mol. Biol.* 235 (1994) 1271–1277.
- [32] S.J. Winder, T.J. Gibson, J. Kendrick-Jones, Dystrophin and utrophin: the missing links! *FEBS Lett.* 369 (1995) 27–33.

- [33] S. Legardinier, J.F. Hubert, O. Le Bihan, C. Tascon, C. Rocher, C. Raguene-Nicol, A. Bondon, S. Hardy, E. Le Rumeur, Sub-domains of the dystrophin rod domain display contrasting lipid-binding and stability properties, *Biochim. Biophys. Acta* 1784 (2008) 672–682.
- [34] N. Greenfield, G.D. Fasman, Computed circular dichroism spectra for the evaluation of protein conformation, *Biochemistry* 8 (1969) 4108–4116.
- [35] B. Berge, A. Renault, Ellipsometry study of 2D crystallization of 1-alcohol monolayers at the water surface, *Europhys. Lett.* 21 (1993) 773–777.
- [36] C. Bottier, J. Gean, B. Desbat, A. Renault, D. Marion, V. Vie, Structure and orientation of puroindolines into wheat galactolipid monolayers, *Langmuir* 24 (2008) 10901–10909.
- [37] L. Chieze, V.M. Bolanos-Garcia, M. Pinot, B. Desbat, A. Renault, S. Beaufiles, V. Vie, Fluid and condensed ApoA-I/phospholipid monolayers provide insights into ApoA-I membrane insertion, *J. Mol. Biol.* 410 (2011) 60–76.
- [38] Y. Zhang, I-TASSER server for protein 3D structure prediction, *BMC Bioinforma.* 9 (2008) 40.
- [39] B. Legrand, E. Giudice, A. Nicolas, O. Delalande, E. Le Rumeur, Computational study of the human dystrophin repeats: interaction properties and molecular dynamics, *PLoS One* 6 (2011) e23819.
- [40] T.V. Pyrkov, A.O. Chugunov, N.A. Krylov, D.E. Nolde, R.G. Efremov, PLATINUM: a web tool for analysis of hydrophobic/hydrophilic organization of biomolecular complexes, *Bioinformatics* 25 (2009) 1201–1202.
- [41] N.A. Baker, D. Sept, S. Joseph, M.J. Holst, J.A. McCammon, Electrostatics of nanosystems: application to microtubules and the ribosome, *Proc. Natl. Acad. Sci. U.S.A.* 98 (2001) 10037–10041.
- [42] R.I. MacDonald, E.V. Pozharski, Free energies of urea and of thermal unfolding show that two tandem repeats of spectrin are thermodynamically more stable than a single repeat, *Biochemistry* 40 (2001) 3974–3984.
- [43] G.C. Chen, J.P. Kane, Circular dichroism of lipoprotein lipids, *Methods Enzymol.* 128 (1986) 519–527.
- [44] N.E. Zhou, C.M. Kay, R.S. Hodges, Synthetic model proteins. Positional effects of interchain hydrophobic interactions on stability of two-stranded alpha-helical coiled-coils, *J. Biol. Chem.* 267 (1992) 2664–2670.
- [45] Y. Desfougeres, A. Saint-Jalmes, A. Salonen, V. Vie, S. Beaufiles, S. Pezennec, B. Desbat, V. Lechevalier, F. Nau, Strong improvement of interfacial properties can result from slight structural modifications of proteins: the case of native and dry-heated lysozyme, *Langmuir* 27 (2011) 14947–14957.
- [46] P. Calvez, S. Bussieres, D. Eric, C. Saless, Parameters modulating the maximum insertion pressure of proteins and peptides in lipid monolayers, *Biochimie* 91 (2009) 718–733.
- [47] V. Vié, N. Van Mau, E. Lesniewska, J.P. Goudonnet, F. Heitz, C. Le Grimellec, Distribution of ganglioside GM1 between two-component, two-phase phosphatidylcholine monolayers, *Langmuir* 14 (1998) 4574–4583.
- [48] N. Jamin, J.M. Neumann, M.A. Ostuni, T.K. Vu, Z.X. Yao, S. Murail, J.C. Robert, C. Giatzakis, V. Papadopoulos, J.J. Lacapere, Characterization of the cholesterol recognition amino acid consensus sequence of the peripheral-type benzodiazepine receptor, *Mol. Endocrinol.* 19 (2005) 588–594.
- [49] J. Sarkis, J.F. Hubert, B. Legrand, E. Robert, A. Cheron, J. Jardin, E. Hitti, E. Le Rumeur, V. Vie, Spectrin-like repeats 11–15 of human dystrophin show adaptations to a lipidic environment, *J. Biol. Chem.* 286 (2011) 30481–30491.
- [50] C. DeWolf, P. McCauley, A.F. Sikorski, C.P. Winlove, A.I. Bailey, E. Kahana, J.C. Pinder, W.B. Gratzner, Interaction of dystrophin fragments with model membranes, *Biophys. J.* 72 (1997) 2599–2604.
- [51] E. Le Rumeur, J.F. Hubert, S.J. Winder, A new twist to coiled coil, *FEBS Lett.* 586 (2012) 2717–2722.
- [52] S. Manno, Y. Takakuwa, N. Mohandas, Identification of a functional role for lipid asymmetry in biological membranes: phosphatidylserine–skeletal protein interactions modulate membrane stability, *Proc. Natl. Acad. Sci. U. S. A.* 99 (2002) 1943–1948.
- [53] R. Saxena, A. Chattopadhyay, Membrane cholesterol stabilizes the human serotonin(1A) receptor, *Biochim. Biophys. Acta* 1818 (2012) 2936–2942.
- [54] A. Ciana, C. Balduini, G. Minetti, Detergent-resistant membranes in human erythrocytes and their connection to the membrane–skeleton, *J. Biosci.* 30 (2005) 317–328.
- [55] M. Grzybek, A. Chorzalska, E. Bok, A. Hryniewicz-Jankowska, A. Czogalla, W. Diakowski, A.F. Sikorski, Spectrin–phospholipid interactions. Existence of multiple kinds of binding sites? *Chem. Phys. Lipids* 141 (2006) 133–141.
- [56] D.D. Doyle, G. Goings, J. Upshaw-Earley, S.K. Ambler, A. Mondul, H.C. Palfrey, E. Page, Dystrophin associates with caveolae of rat cardiac myocytes: relationship to dystroglycan, *Circ. Res.* 87 (2000) 480–488.
- [57] H.M. McConnell, A. Radhakrishnan, Condensed complexes of cholesterol and phospholipids, *Biochim. Biophys. Acta Biomembr.* 1610 (2003) 159–173.
- [58] J.R. Silvius, Role of cholesterol in lipid raft formation: lessons from lipid model systems, *Biochim. Biophys. Acta Biomembr.* 1610 (2003) 174–183.
- [59] A. Radhakrishnan, H.M. McConnell, Electric field effect on cholesterol–phospholipid complexes, *Proc. Natl. Acad. Sci. U. S. A.* 97 (2000) 1073–1078.
- [60] J.R. Silvius, Cholesterol modulation of lipid intermixing in phospholipid and glycosphingolipid mixtures. Evaluation using fluorescent lipid probes and brominated lipid quenchers, *Biochemistry* 31 (1992) 3398–3408.
- [61] J.A. Killian, Hydrophobic mismatch between proteins and lipids in membranes, *Biochim. Biophys. Acta* 1376 (1998) 401–415.
- [62] R. Phillips, T. Ursell, P. Wiggins, P. Sens, Emerging roles for lipids in shaping membrane–protein function, *Nature* 459 (2009) 379–385.
- [63] R.M. Epand, A. Thomas, R. Brasseur, R.F. Epand, Cholesterol interaction with proteins that partition into membrane domains: an overview, *Subcell. Biochem.* 51 (2010) 253–278.
- [64] C.H. Lai, C.K. Lai, Y.J. Lin, C.L. Hung, C.H. Chu, C.L. Feng, C.S. Chang, H.L. Su, Characterization of putative cholesterol recognition/interaction amino acid consensus-like motif of *Campylobacter jejuni* cytolethal distending toxin C, *PLoS One* 8 (2013) e66202.